RSC Advances

PAPER

View Article Online
View Journal | View Issue

Cite this: *RSC Adv.*, 2025, **15**, 18392

Development of a semiconducting supramolecular copper(II)–metallogel for antimicrobial and microelectronic device applications†

Sangita Some,[a] Pubali Das,[b] Suchetana Pal,[c] Subhendu Dhibar,*[a] Dimpal Kumari,[d] Subham Bhattacharjee,[e] Soumya Jyoti Ray,[d] Timothy O. Ajiboye,[f] Somasri Dam,*[c] Partha Pratim Ray*[b] and Bidyut Saha*[a]

A novel supramolecular metallogel was synthesized at room temperature using copper(II) acetate and isophthalic acid as gelators in *N*,*N*-dimethylamine. Rheological studies demonstrated the metallogel's robust mechanical stability under diverse conditions. FESEM imaging and EDX mapping provided detailed insights into its microstructure and elemental composition. The formation of the metallogel was confirmed through FT-IR spectroscopy, which highlighted the successful coordination between the metal ion and the organic ligand. Electrical property analysis revealed its semiconducting nature with impressive conductivity. Additionally, antimicrobial studies showed that the Cu(II)-based metallogel exhibited significant efficacy against Gram-positive and Gram-negative bacteria, making it a promising candidate for combating bacterial infections. These findings establish the developed metallogel as a versatile multifunctional material with dual applicability in electronics and biomedicine. Furthermore, its semiconducting properties suggest its potential integration into advanced electronic devices, while its antimicrobial activity highlights its potential in medical treatments. This study underscores the potential of Cu(II)–isophthalic acid-based metallogels, combining mechanical resilience, electrical conductivity, and antimicrobial efficacy to address various critical technological and biomedical challenges.

Received 4th March 2025
Accepted 20th May 2025

DOI: 10.1039/d5ra01535a

rsc.li/rsc-advances

1. Introduction

A gel is a colloid system consisting of a liquid as the dispersed phase and solid as the dispersed medium. It is a typically semi-solid, three-dimensional (3D) crosslinked polymeric network formed *via* the immobilization of solvent molecules.[1] The spontaneous production of gels makes their synthesis and design intriguing and unpredictable.[2] The vial inversion test under the force of gravity is the primary technique for identifying a mixture as gel, with rheological analysis used to confirm gel formation.[3]

Gels may be categorised into two types, namely, chemical gels, formed *via* rapid covalent bonding interactions, and supramolecular gels, composed of self-assembled,[4] low molecular gelator (LMWG) molecules,[3,4] with a molecular weight less than 3000 and formed through various non-covalent interactions,[5] such as hydrogen bonding,[6] π···π stacking interaction, and van der Waal forces.[7,8] LMWGs have recently attracted attention owing to their ability to produce nanostructures in supramolecular gels in addition to their gelation activity.[2] The regulation of the nanostructure can be achieved by selecting appropriate gelators[9] and solvents.[10] Dibasic acids,[11] amides,[12] amines,[13] carbohydrates,[14] and amino acid derivatives[15] are effective gelators for the synthesis of supramolecular gels.[16] Rigid aromatic crosslinkers, such as those containing benzene rings or polycyclic aromatic systems (*e.g.*, benzophenone and bisphenol derivatives), can impart enhanced mechanical strength, improved thermal stability, and, often, better conductivity to metallogels. The rigid nature of these linkers restricts rotational freedom, thereby facilitating stronger π···π stacking interactions and the formation of more ordered supramolecular networks. For example, isophthalic acid and its amino derivatives, including 2-amino terephthalic acid and 5-aminoisophthalic acid, have been widely employed in metallogel systems because of their efficient coordination capabilities with metal ions and structural rigidity. Notably, Dey *et al.* (2023)

[a]*Colloid Chemistry Laboratory, Department of Chemistry, The University of Burdwan, Golapbag, Burdwan 713104, West Bengal, India. E-mail: sdhibar@scholar.buruniv.ac.in; bsaha@chem.buruniv.ac.in; Tel: +91 7001575909; +91 9476341691*

[b]*Department of Physics, Jadavpur University, Jadavpur, Kolkata 700032, India. E-mail: parthap.ray@jadavpuruniversity.in; Tel: +91 3324572844*

[c]*Department of Microbiology, The University of Burdwan, Burdwan 713104, West Bengal, India. E-mail: sdam@microbio.buruniv.ac.in*

[d]*Department of Physics, Indian Institute of Technology Patna, Bihar 801106, India*

[e]*Department of Chemistry, Kazi Nazrul University, Asansol 713303, West Bengal, India*

[f]*Department of Chemistry, University of the Free State, Bloemfontein, 9301, South Africa*

† Electronic supplementary information (ESI) available. See DOI: https://doi.org/10.1039/d5ra01535a

reported an Mn(II)-based metallogel[17] using 2-amino terephthalic acid for Schottky diode applications, and Dhibar *et al.* (2023) reported the use of 5-aminoisophthalic acid to fabricate Zn(II),[18] Ni(II),[19] and Co(II)[20] metallogels, which showed promising performance for semiconducting and microelectronic device applications. In contrast, flexible linkers, such as those based on aliphatic chains or ether-containing moieties (*e.g.*, polyethylene glycol and aliphatic diamines), offer greater conformational freedom.[21,22] These systems typically exhibit lower mechanical rigidity but enhanced flexibility, dynamic responsiveness, and self-healing behaviour. Such linkers are more suitable for applications requiring reversible structural changes or stimuli-responsive functions. Another essential factor in initiating gel formation is the solvent.[23] In particular, the polarity and viscosity of the solvent may alter the gel morphology.[24] The use of specific type of gelators determines whether inorganic or organic solvents will be effective for promoting gel formation.[25] The most effective solvents for starting a supramolecular gel are water,[26] alcohols,[27] dimethyl formamide,[28] dimethyl sulfoxide,[29] 1,2-dichlorobenzene,[30] acetonitrile,[31] acetone,[32] toluene,[33] dichloromethane,[34] and deuterated dichloromethane.[35] Reports have demonstrated that reversible gel-to-sol phase transition[36,37] can be brought about by its weak non-covalent interactions[37] and under the influence of different external mechanical forces, pH, temperature, electrolytes, *etc.*[38] Supramolecular gels have intriguing potential a range of applications in diverse fields, such as drug delivery,[39] scaffolds for tissue regeneration,[40] transporters for therapeutic medications,[41] catalysis,[42] soft robotics,[43] pollutants absorption,[44] and the controlled release of chemicals into the environment.[45]

Metal ions or metal complexes can self-assemble with organic ligands (LMWGs) to form 3D networks known as supramolecular metallogels, a kind of supramolecular gel.[46] These gels are held together by coordination bonding interactions between the metal centers and the ligands, in addition to other non-covalent interactions, including hydrogen bonding,[7] π–π stacking,[47] and van der Waals forces.[9] By selecting different metal ions and ligands and altering the surrounding environment, the properties of the supramolecular metallogels may be changed.[47,48] Scientists are interested in transition metal-based metallogels because of their accessibility, affordability, and improved capacity to coordinate with organic ligands. Peptide nanofibers integrated with silver nanoparticles have been explored as a potential antimicrobial nanohybrid gel.[49] Copper is an essential trace element for many cellular functions, but it can also have a toxic impact by triggering ROS generation. The exposure of copper sulfate to HeLa cells led to a decrease in cell viability, increase in the sub G1 and G2/M populations, and the upregulation of autophagy, senescence, mitochondrial dysfunction, and ROS generation.[49] Copper(II) ions are often selected as an excellent metal for metallogel synthesis due to their variable oxidation states,[14] coordinating versatility,[20] redox activity,[28] cost effectiveness[4] and biomedical activities.[41] In semiconducting devices, the extended π-conjugation and charge-transfer capabilities of Cu(II) centers enhance the charge-carrier mobility and electrical conductivity, making them promising candidates for use in flexible electronics and second-generation Schottky barrier diodes.[50,51] Concurrently, the intrinsic antimicrobial activity of Cu(II) ions, driven by their ability to generate reactive oxygen species and disrupt microbial membranes, imparts excellent antibacterial properties to metallogels they are included in, broadening their utility in biomedical and environmental applications. Indeed, copper metallogels have attracted a lot of interest because of their special blend of qualities. Among their significant applications are catalysis,[42] antimicrobial materials,[41] energy storage,[43] sensors,[47] environmental remediation,[44] and soft electronics.[49] Dicarboxylic acids are other materials that are useful in metallogel research.[52,53] Because of their carboxylate groups,[54–64] they can interact with transition metals and form coordination complexes that facilitate gelation. In previous studies, gels mediated by succinic, oxalic and adipic acids have been reported with specific uses and with minimal levels of toxicity.[51]

Metallogel-based Schottky diodes offer significant promise across a wide range of applications as they offer several key advantages. By selecting specific metals and organic ligands during their synthesis, the precise tuning of their electronic properties can be achieved, including control over their energy band structure and ultimately device performance. Their robust stability ensures their long-term reliability, even under varying environmental conditions. Additionally, metallogels can be fabricated through multiple methods, such as solution processing, self-assembly, and templating, offering flexibility for integration with diverse substrates and scalable manufacturing. Their compatibility with other electronic components, including transistors and sensors, further supports the creation of multifunctional, high-performance devices. Collectively, their many beneficial features, including tunable electronic behaviour, high durability, versatile fabrication, and material compatibility,

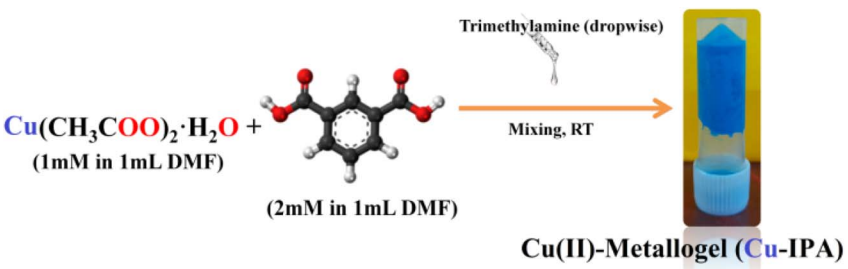

Fig. 1 Synthesis of the Cu-IPA metallogel and a photograph of the metallogel in a vial that has been inverted.

make metallogel-based Schottky diodes highly attractive for advanced electronic and optoelectronic applications.

In a notable contribution, Dhibar and co-workers[4,5,8,14,18] introduced a simple and efficient synthesis route for metallogels, which enabled avoiding harsh reaction conditions while maintaining their functionality. Their work demonstrated the adaptability of metallogel systems for next-generation semiconductor devices. Following this direction, we developed a room-temperature-stable metallogel using copper(II) ions and isophthalic acid as a low molecular weight gelator (LMWG) in *N*,*N*-dimethylformamide (DMF) (Fig. 1). The resulting Cu(II)–metallogel, termed Cu-IPA, showed excellent mechanical strength, as confirmed through the inverted vial test (Fig. 1). Further detailed morphological studies were conducted on the material. Also, a Schottky barrier diode (SD) was successfully fabricated using this material to demonstrate its application potential in an important area. Beyond its electronic applications, Cu-IPA also displayed strong antibacterial activity against both Gram-positive and Gram-negative bacteria, highlighting its multifunctional potential.

2. Experimental section

2.1. Materials

Copper(II) acetate monohydrate (99% extra pure) and isophthalic acid (99% extra pure) were purchased from SRL and used as received. Throughout the study, dry DMF solvent was utilized. Commercially available DMF (purchased from SRL) was dried using calcium hydride (~1.5 g/100 mL) for 6 h at room temperature. After the drying process, the intermediate fraction was collected and kept on activated molecular sieves to preserve its anhydrous condition. Yeast extract powder, tryptone and D-(+)-glucose anhydrous were purchased from Himedia. The acetone and ethanol used in the device fabrication were of analytical reagent (AR) grade with a purity of ≥99.5%, and were procured from Sigma-Aldrich. Distilled water was freshly prepared in the laboratory using double-distillation apparatus.

2.2. Apparatus and measurements

2.2.1 UV-visible spectroscopy analysis. An Avaspec-2048 UV-visible spectrometer was used to analyse the UV-vis absorption spectra of the metallogel.

2.2.2 Rheological analysis. The rheology experiments were performed with fixing the gap distance between the cone and the plate as 0.5 mm. The gels were scooped on to the plate of the rheometer. An oscillatory strain amplitude sweep experiment was performed at a constant oscillation frequency of 1 Hz for the applied strain range of 0.001–100% at 25 °C. Oscillatory frequency sweep experiments were performed in the linear viscoelastic region (strain of 0.01%) to ensure that calculated parameters corresponded to intact network structures.

2.2.3 Field emission scanning electron microscopy (FESEM) study. The metallogel samples were carefully drop-cast on top of the freshly cleaned glass surface and allowed to air-dry overnight. The samples were then coated with gold vapor and analyzed on a Carl Zeiss SUPRA 55VP instrument operated at 10–15 kV, while a ZEISS EVO 18 device was used for the energy-dispersive X-ray spectroscopy (EDX) investigations.

2.2.4 FT-IR study. The IR spectra were recorded in the 4000–500 cm^{-1} range for the samples pelleted in KBr using a JASCO FT-IR 4700 spectrophotometer.

2.2.5 Electrical study. A Keithley 2400 source meter that was linked to a computer was used to record the device's IV parameters.

2.3. Synthesis of the Cu(II)–metallogel using isophthalic acid as a gelator

Copper(II) acetate monohydrate was used to effectively synthesize a blue-colored metallogel based on isophthalic acid at room temperature (RT). In a single step, 1 mL DMF solution containing 0.332 g (2 mmol) of isophthalic acid and 0.200 g (1 mmol) of copper(II) acetate monohydrate in 1 mL DMF were combined in the presence of 0.2 mL trimethylamine base.

2.4. Evaluation of the minimum critical gelation concentration (MGC)

The assessment of the minimum critical gelation concentration (MGC) of the Cu-IPA metallogel is presented in Fig. 1, showing the result of the vial inversion test. The concentrations of $Cu(CH_3COO)_2 \cdot H_2O$ and isophthalic acid were varied in a certain range (*i.e.*, 30–532 mg mL^{-1}) to evaluate the MGC of the Cu-IPA metallogel. Herein, the ratio of the Cu-IPA metallogel forming components was maintained as $[Cu(CH_3COO)_2 \cdot H_2O]$: [isophthalic acid] = 1 : 2, (w/w). The stable and blue-colored metallogel Cu-IPA metallogel was obtained at 532 mg mL^{-1} concentration of Cu(II)–acetate salt and isophthalic acid combined in the presence of 0.2 mL of trimethylamine base in DMF solvent.

2.5. Antimicrobial activity of Cu-IPA

The susceptibility of bacterial strains to the metallogel Cu-IPA was assessed. A 100 mg per mL metallogel suspension was prepared in deionized water (Merck Millipore, France). The antibacterial efficacy was assessed against Gram-positive bacteria, *i.e.*, *Bacillus subtilis* (*B. subtilis*), *Staphylococcus epidermidis* (*S. epidermidis*), and Gram-negative bacteria, *i.e.*, *Escherichia coli* (*E. coli*), and *Pseudomonas aeruginosa* (*P. aeruginosa*). A common broad-range antibiotic, *Streptomycin*, served as a positive control in the experiment. TGE (tryptone, glucose, yeast extract, all at 1%; pH 6.5) agar was used as the growth medium. Then, 100 μL of each bacterial inoculum in its logarithmic growth phase was spread across the agar medium using sterile cotton swabs. Next, 10 μL of the metallogel suspension was spotted on the surface of the medium. The plates were then incubated at 37 °C for 24 h. The experiments were carried out in triplicate.

2.6. Device fabrication

For measuring the electrical properties of material itself and its performance in device applications, a metal–semiconductor (MS) junction was fabricated, wherein the synthesized material acted as a semiconductor (Scheme 1). For this very purpose, initially

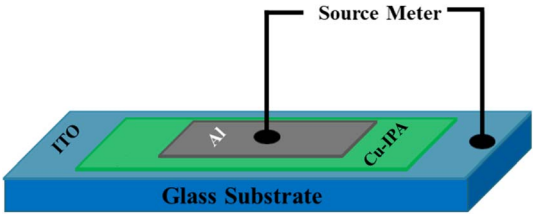

Scheme 1 Schematic representation of the fabricated metal–semiconductor (MS) junction device utilizing the Cu-IPA metallogel.

a glass substrate covered with indium tin oxide (ITO) was meticulously cleansed using acetone, ethanol, and distilled water in a sequential manner with the aid of an ultrasonicator. Next, the substrate was dried under a nitrogen (N_2) atmosphere. The metallogel was then applied on the pre-cleaned ITO-coated glass with the doctors' blade method followed by naturally drying in a vacuum chamber to obtain a homogenous thin film of the metallogel. The film thickness (d) was measured as being around 1 μm using a surface profiler. Finally, an electron beam gun was employed to apply aluminium metal onto the film under a base pressure of 10^{-6} torr. The effective diode area (A) was maintained at 7.065×10^{-6} m^2 using a pre-cleaned shadow mask.

3. Results and discussion

3.1. Fourier transform infrared (FT-IR) analysis of Cu-IPA metallogel

Fourier transform infrared (FT-IR) spectroscopy is good at identifying different functional groups, hence it was used herein to investigate the produced Cu-IPA metallogel. The supramolecular interactions between isophthalic acid and Cu(II) sources that propel the metallogel's production were visible in the FT-IR spectrum in the xerogel form of the Cu-IPA metallogel (Fig. 2). The FT-IR spectrum revealed distinct peak shifts at 1370 and 3397 cm^{-1}, which were indicative of the vibrational signatures associated with copper acetate, confirming its presence within the metallogel matrix. Moreover, additional absorption bands could be observed at 684, 1270, 1612, 1670 and 2972 cm^{-1}, which were consistent with the vibrational modes of isophthalic acid, thereby supporting its successful incorporation into the gel framework. A large peak at 3397 cm^{-1}, which corresponded to the O–H stretching[52] of hydroxyl groups, was one of the key absorption bands of the Cu-IPA metallogel. The carboxyl C=O stretching appeared as a peak at 1670 cm^{-1}, while the vibrational mode observed at 2972 cm^{-1} was associated with symmetric C–H bonds.[53] C–N stretching[54] and C–O stretching[55] were represented by the additional vibrational modes seen at 1370 and 1270 cm^{-1} respectively. The asymmetric and symmetric stretching bands of the COO^- group in copper acetate, originally observed at 1550 and 1450 cm^{-1}, respectively, were shifted to 1623 and 1384 cm^{-1} after metallogel formation. The change in $\Delta\nu$ (COO), *i.e.*, (ν_{as}–ν_s), strongly suggested the replacement of acetate ions, which freed the metal ion and allowed it to bind with isophthalic acid. Moreover, the broad O–H stretching band of (IPA), ranging from 2360 to 3000 cm^{-1}, completely disappeared after metallogel formation. This indicates the deprotonation of the –COOH groups and the formation of $–COO^-$ groups, which then coordinate with the metal center. The appearance of a peak

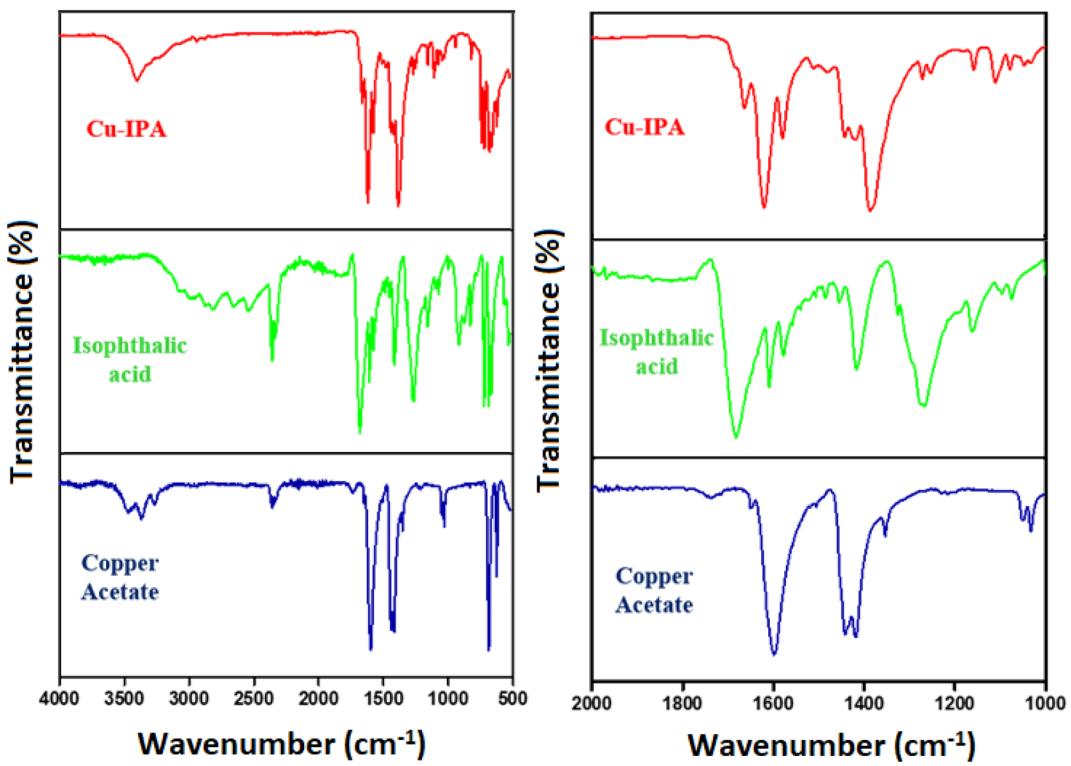

Fig. 2 FT-IR spectra of the Cu-IPA metallogel in xerogel form, isophthalic acid, and copper acetate.

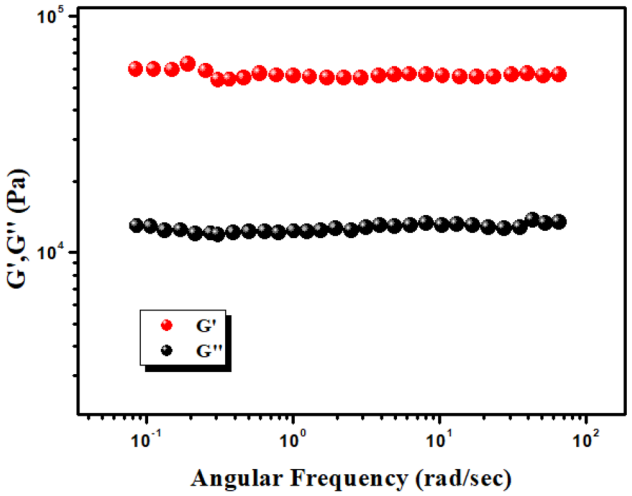

Fig. 3 Angular frequency measurements *vs.* G' and G'' of the Cu-IPA metallogel.

at 750 cm^{-1} provides evidence for the presence of the aromatic ring of isophthalate. Additionally, the aromatic C=C stretching band around 1600 cm^{-1} served as a diagnostic peak for the isophthalate used as a gelator in the metallogel network. Additionally, the peak at 684 cm^{-1} confirmed the presence of Cu–O bonds, indicating the effective connection between DMF-soluble copper acetate and isophthalic acid. The distinct Cu–O stretching vibration observed at 684 cm^{-1}, along with the presence of prominent C=O (1670 cm^{-1}) and C–O (1270 cm^{-1}) stretching bands, provided evidence for the conversion of copper acetate to copper isophthalate in the metallogel network.

3.2. Rheological analysis

The mechanical properties of the Cu-IPA metallogel were investigated by rheological analysis, specifically angular frequency and strain–sweep measurements. The gel nature of the Cu-IPA metallogel was confirmed by the observation that its storage modulus (G') consistently exceeded its loss modulus (G''). Indeed, these measurements, conducted at a fixed concentration of $Cu(CH_3COO)_2 \cdot H_2O$ and isophthalic acid corresponding to the minimum gelation concentration (MGC) of 532 mg mL^{-1}, demonstrated the significant dominance of the storage modulus (G') over the loss modulus (G''), as shown in Fig. 3. The results affirmed the semi-solid, gel-like nature of the Cu-IPA metallogel. Notably, the average storage modulus (G') exceeded 10^2 Pa, substantially surpassing the loss modulus (G''), further supporting the robust gel network and its mechanical stability (Fig. 3). The results of the strain–sweep experiments with the Cu-IPA metallogel are provided in Fig. S1 in the ESI.†

3.3. Microstructural study

A network structure resembling flake-like formations could be observed in the field emission scanning electron microscopy (FESEM) images of the metallogel (Fig. 4a and b). The FESEM images clearly show the complex structure, which was made from $Cu(CH_3COO)_2 \cdot H_2O$ and isophthalic acid in DMF medium. The dominant supramolecular interactions, which are essential for the formation of the Cu-IPA metallogel, were probably the source of the microstructural network. The existence of copper acetate and isophthalic acid, which are crucial elements in the composition of the metallogel, was verified by elemental mapping of a particular area inside the gel. The existence of carbon (C), nitrogen (N), oxygen (O), and copper (Cu) components was confirmed by energy-dispersive X-ray spectroscopy (EDX), as displayed in Fig. 4c–g, which verified that $Cu(CH_3COO)_2 \cdot H_2O$, isophthalic acid, and DMF had been successfully integrated into the metallogel framework.

3.4. Dielectric properties

The dielectric characteristics of any solid material are contingent upon the distribution of the local electric field within the system. Understanding the dielectric characteristics can provide valuable insights into the charge-transport process and structural alterations in a solid material. The dielectric properties of the produced material were analysed using impedance

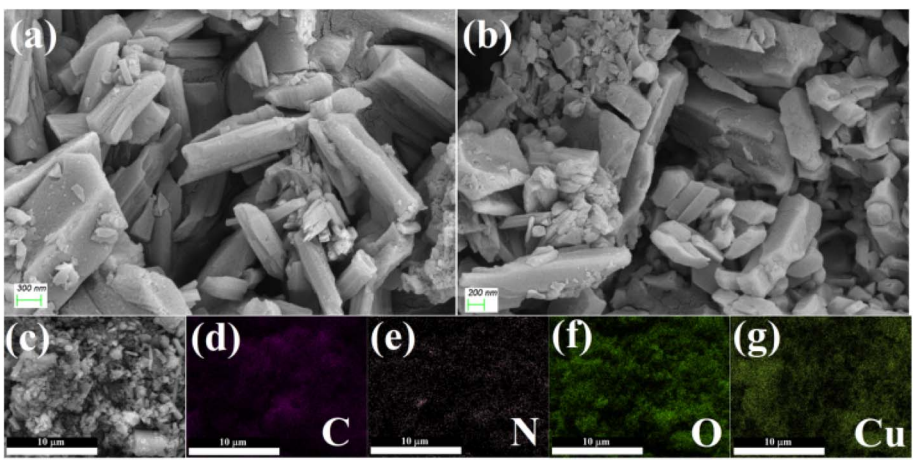

Fig. 4 (a and b) FESEM microstructural analysis of the metallogel; (c–g) elemental analysis showing the presence of C, N, O, and Cu.

spectroscopy within the frequency range of 40 Hz to 10 MHz. The experiments were conducted under ambient conditions. The optical property of the Cu-IPA metallogel is shown in Fig. S2 in the ESI.†

The dielectric property exhibited a complex nature when subjected to an alternating current (AC) field.

The total dielectric constant is given by the following equation,[30]

$$\varepsilon = \varepsilon' - j\varepsilon'' \quad (1)$$

where ε' is the real part and ε'' is the imaginary part of the dielectric constant. The real part stands for the energy storage in a material while the imaginary part describes the energy dissipation in the material.

The real and imaginary part of the dielectric constant of the material can be determined from the following equations,[65]

$$\varepsilon' = \frac{d}{\varepsilon_0 \times \omega \times A} \times \frac{Z_m''}{Z_m'^2 + Z_m''^2} \quad (2)$$

and

$$\varepsilon'' = \frac{d}{\varepsilon_0 \times \omega \times A} \times \frac{Z_m'}{Z_m'^2 + Z_m''^2} = \varepsilon' \tan\delta \quad (3)$$

where ε_0 is the free space permittivity, d denotes the thickness of the film, A is the surface area of the film, Z_m' is the real impedance, Z_m'' indicates the imaginary impedance of the metallogel, and tan δ specifies the dielectric loss tangent.

The dielectric characteristics of the Cu-IPA-metallogel can be affected by several parameters, including the manufacturing technique, chemical composition, ionic charge, and grain size.

Fig. 5 shows that the dielectric constant and dielectric loss factor decreased rapidly as the frequency increased, until they reached a constant value at higher frequencies. This occurs because the electron–exchange interaction (hopping) between the Cu^+ and Cu^{2+} ions is unable to keep up with the alternating ac electric field beyond a certain critical frequency.

Fig. 5a shows the variation of the real part of the dielectric (dielectric constant) with frequency for the metallogel. A hopping model considering the sample as an integration of a large number of dipoles is best to describe the behaviour displayed in the figure and the above drawn conclusion. In this model, at low frequencies the alternating current field remains slow, and the dipoles have adequate time to align themselves with the direction of the applied field, which enhances the polarization. On the other hand, the diminution in the value at higher frequencies can be explained by the phenomenon of dipole relaxation. In the high-frequency zone, the dipoles become unable to rapidly change their orientation, causing their oscillation to fall behind the alternating current (ac) field. Therefore, the dielectric constant dropped as a result of the random alignment of dipoles. The observed dispersion mostly arose from the interfacial Maxwell–Wagner-type polarisation, consistent with Koop's phenomenological theory.[66,67]

The dielectric loss factor, *i.e.*, the imaginary part, represents the dissipation of energy in the system. Fig. 5b presents the dielectric loss of the synthesized metallogel as a function of frequency at room temperature. Dielectric loss occurs when the charge carriers in a dielectric system are unable to respond to changes in the electric field. Increasing the frequency of the applied field results in lower dielectric losses. This phenomenon is likely caused by the suppression of domain walls, resulting in a compelled alteration of the magnetisation rotation. At higher frequencies, a reduced tangential loss (Fig. 5a) can also indicate the presence of Maxwell–Wagner relaxation[68] It is evident from Fig. 5b and 6a that there was a direct correlation between lower frequencies and increased dielectric loss. The presence of space-charge polarisation at lower frequencies can be attributed to the Shockley–Read process.[68]

Fig. 6 displays the ac conductivity of the metallogel with respect to frequency. The ac conductivity can be determined by the following equation,[69]

$$\sigma_{ac} = \frac{Z_m'}{Z_m'^2 + Z_m''^2} \cdot \frac{d}{A} \quad (4)$$

It can be clearly observed from the ac conductivity graph, that after a certain value of frequency the conductivity became independent of the frequency. The ac conductivity can be expressed by the following equation, using Jonscher's law,[70]

$$\sigma_{ac} = \sigma_{dc} + C\omega^n \quad (5)$$

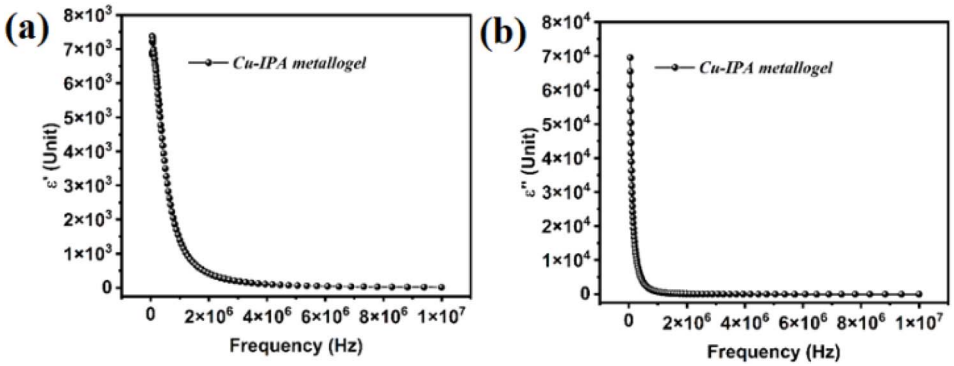

Fig. 5 (a) Dielectric constant *versus* frequency graph and (b) imaginary part of dielectric *versus* frequency graph for the as-synthesized metallogel.

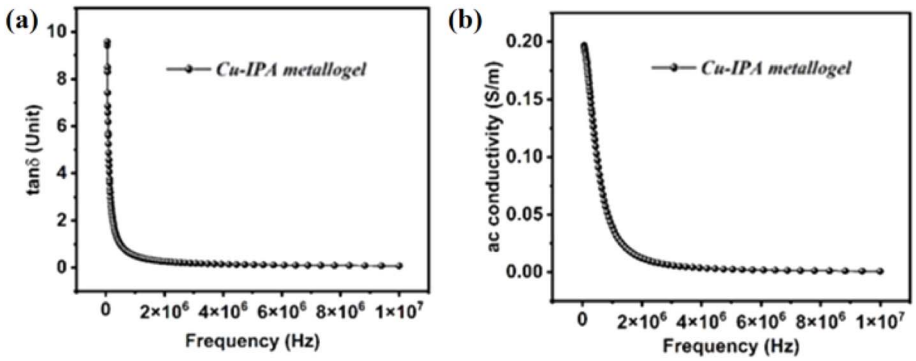

Fig. 6 (a) Tangential loss *versus* frequency graph and (b) ac conductivity graph of the metallogel.

where σ_{dc} is the frequency-independent conductivity or dc conductivity, C is a coefficient, ω is the angular frequency of the electric field and n is the exponent ($0 \leq n \leq 1$). When the value of n is less than or equal to 1, a sudden hopping occurs, which leads to the engagement of both hopping conduction and translational motion.

From eqn (5) and Fig. 6b, it is obvious that the frequency-independent part of the ac conductivity graph extrapolated to the ac conductivity axis gives the value of σ_{dc}. The evaluated value of dc conductivity for the as-synthesized metallogel was 5.49×10^{-3} S m^{-1}.

The value of the metallogel's dc conductivity suggests an obvious semiconducting behaviour, leading to an approach towards a metal–semiconductor junction formation.

However, in the low-frequency region in the graph, the ac conductivity decreased rapidly with the increase in frequency up to a certain range of frequency. As is already known, the resistance and inductive reactance have a positive correlation with frequency, whereas the capacitive reactance has a negative correlation with frequency,[71] and conductivity decreases with the increase in resistance, wherein the possibility of a more resistive part in the metallogel than capacitive part can well describe this fact.

3.5. Electrical characterization

A device was fabricated with the structure Al/Cu-IPA-metallogel/ITO, and used to probe to a range of bias voltages from −1 V to +1 V, and the associated current values were measured.

Fig. 7 depicts the current of the formed diode as it varied with the applied bias, presented in two distinct current scales. The *I*–*V* curve demonstrated nonlinearity, which validated the presence of Schottky barriers at the metal–semiconductor (MS) junction, with a rectification ratio of 69.88. Thermionic emission theory was applied to analyse the recorded *I*–*V* data for further determination of the diode parameters, with this described in the ESI.†

The correlation between the natural logarithm of the current and the natural logarithm of the applied forward bias voltage is depicted in Fig. 8, which can help gain an insight into the carrier-transport mechanism across the interface. The investigation focused on analysing the mechanism that regulates

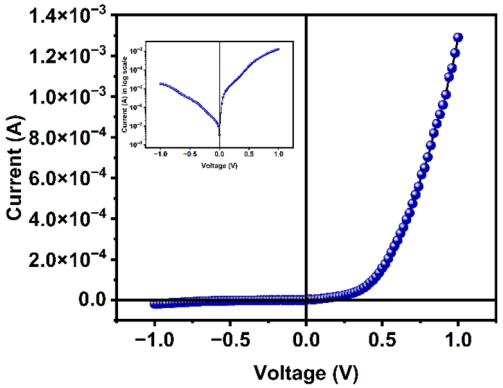

Fig. 7 Current–voltage (*I*–*V*) measurement of the fabricated structure in linear scale; inset shows the same in log scale.

carrier conduction at the Schottky contact, using the slope of the graph as a basis implying the power law ($I \propto V^m$). The slope value (m) of 1, or the direct relationship between current and voltage (Arena I), indicates the charge transport occurs due to ohmic conduction.[72,73]

The conductivity of the formed device was calculated as 1.7×10^{-5} S m^{-1} in this arena of conduction. The ideality factor, barrier height and series resistance of the fabricated device can also be determined from this arena.

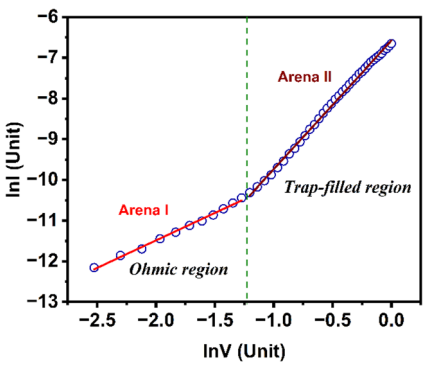

Fig. 8 ln *I versus* ln *V* plots for the Schottky device.

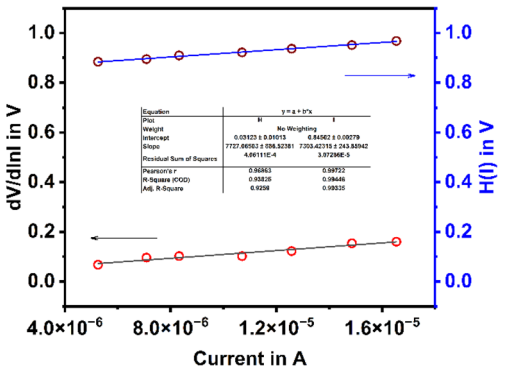

Fig. 9 dV/dln I and $H(I)$ *versus* I for the fabricated Schottky device.

Table 1 Schottky diode parameters

Ideality factor	Barrier height (eV)	R_s from dV/dln I (kΩ)	R_s from $H(I)$ (kΩ)
1.19	0.708	7.7	7.3

For these, the well-known Cheung and Cheung equation derived using the thermionic emission eqn (S1)† was utilized to analyse the recorded I–V data of Arena I.

According to Cheung's model[74]

$$\frac{dV}{d\ln I} = \frac{\eta kT}{q} + IR_s \quad (6)$$

and

$$H(I) = V - \left(\frac{\eta kT}{q}\right)\ln\left(\frac{I}{AA^*T^2}\right) = IR_s + \eta\phi_b \quad (7)$$

where $H(I)$ is a function of the current.

The series resistance and ideality factor (I.F.) were determined by analysing the slope and intercept of the dV/dln I against I curve (Fig. 9), which was fitted linearly (Table 1).

Table 1 includes the barrier height and series resistance values obtained by analysing the intercept and slope of the $H(I)$ *vs.* I graphs. The resistances in the series, acquired by the two different approaches, displayed similar patterns. The deviation of the ideality factor from 1 may be attributed to the presence of tunnelling current, electron and hole recombination in the depletion zone, inhomogeneity at the barrier, or a combination of these variables. The device characteristics are believed to be greatly impacted by the properties of the metal and semiconductor contact, as well as the conditions of the surface.[75]

In Arena II, the slope value was greater than 3. This arena is called the trap-assisted region of the current conduction. The presence of traps near the Fermi level is responsible for this

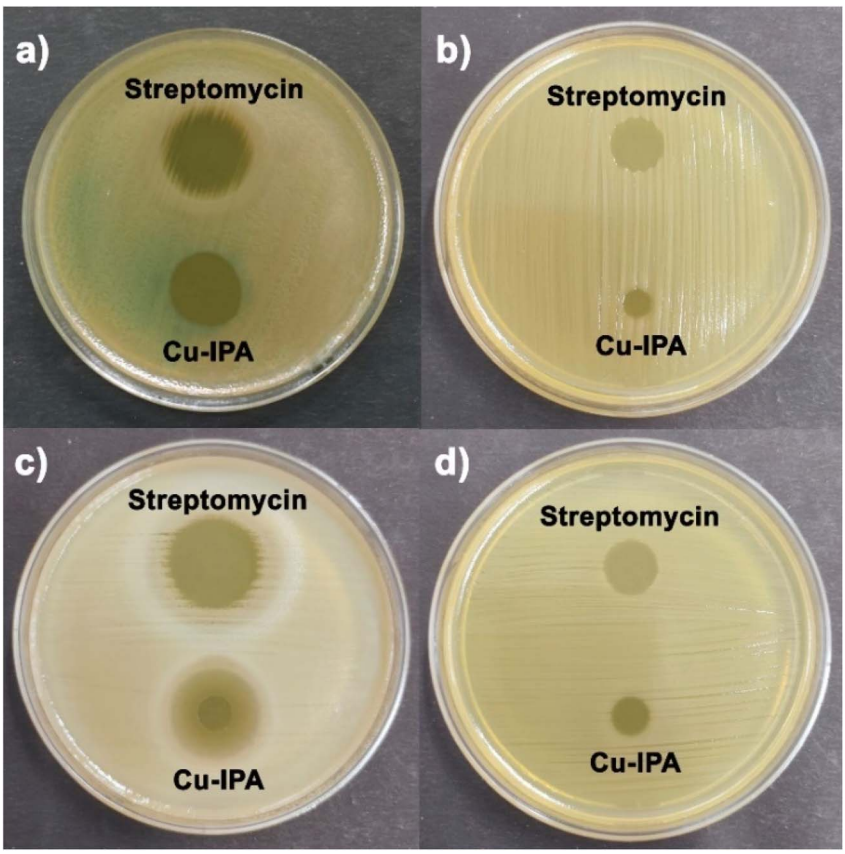

Fig. 10 Antimicrobial activity of Cu-IPA against four pathogenic strains: (a) *P. aeruginosa*, (b) *E. coli* (c) *B. subtilis*, and (d) *S. epidermidis*.

Table 2 Antimicrobial activity of the metallogel[a]

Bacterial strain (s)	Zone of inhibition (mm in diameter) against streptomycin	Concentration of metallogel (mg mL^{-1})	Volume of metallogel given (μL)	Zone of inhibition against Cu-IPA metallogel (mm in diameter)
P. aeruginosa (a)	19.4 ± 0.40	100	10	20.7 ± 0.26
E. coli (b)	13.3 ± 0.28	100	10	7.06 ± 0.11
B. subtilis (c)	21.2 ± 0.25	100	10	21.06 ± 0.11
S. epidermidis (d)	13.2 ± 0.2	100	10	9.16 ± 0.15

[a] ±Standard deviation.

phenomenon. This behaviour can be used to ascertain the distinctive trap energy. The text describes how trap density distribution declines within the forbidden gap below the conduction band edge.[76–80]

3.6. Inhibition activity against pathogens

Cu-IPA exhibited strong antimicrobial activity against Gram-positive *B. subtilis* and *S. epidermidis* and Gram-negative *E. coli* and *P. aeruginosa* (Fig. 10). After being placed in the incubator, the metallogel gradually dispersed throughout the agar medium. The region where the metallogel concentration was sufficiently high to inhibit bacterial growth appeared as a clear, circular zone. The diameter of this zone directly reflected the potency of the metallogel against the tested microorganisms. Synthesized derivatives showing comparable inhibition zones to the control antibiotic are considered as promising antimicrobial agents. Also, a reduced inhibition zone relative to streptomycin does not preclude antimicrobial properties; rather, it suggests a lower potency at the given concentration. This characteristic is beneficial in controlled drug treatment, where a low or moderate level of inhibition is desired. The observed inhibitory effects of Cu-IPA on microorganisms suggested its suitability for a wide range of antimicrobial applications. The antimicrobial efficacy of Cu-IPA on the four aforementioned bacterial strains is presented in Table 2.

4. Conclusions

In summary, a supramolecular Cu(II)-metallogel was successfully synthesized by combining copper (II) acetate monohydrate and isophthalic acid in DMF medium with trimethylamine at room temperature. FESEM analysis revealed a flake-like microstructure, while rheological studies confirmed the metallogel's mechanical robustness. FT-IR spectroscopy elucidated the intermolecular interactions that underpin the gel formation. The semiconducting properties of the metallogel were highlighted through optical band-gap analysis and further validated by the fabrication of a metal–semiconductor junction thin-film device. The ITO/Cu-IPA metallogel/Al sandwich structure exhibited a high rectification ratio and enhanced photosensitivity, demonstrating its potential for applications in optoelectronics and rectification technologies. Moreover, the Cu-IPA metallogel showed strong antibacterial activity, suggesting its significant promise in pharmaceutical and biological applications. The adaptability of the synthesis process enables the customization of material properties for specific needs, which may pave the way for further exploration in material science. This work emphasizes the value of interdisciplinary research in advancing innovative material designs to tackle pressing societal challenges. By integrating Cu(II)-metallogels into practical solutions, this study lays a foundation for advancements in healthcare, environmental protection, and cutting-edge electronics. The findings underline the transformative potential of supramolecular materials in addressing critical technological and biomedical needs.

Data availability

The authors declare that the data supporting the findings of this study are available within the paper and its ESI files.† Should any raw data files be needed in another format, they are available from the corresponding author upon reasonable request.

Conflicts of interest

The authors declare no competing financial interests.

Acknowledgements

S. S. is thankful to DST India, New Delhi, for Inspire Fellowship (No. DST/inspire Fellowship/2022/IF220441).

References

1 D. Tripathy, A. S. Gadtya and S. Moharana, *Polym.-Plast. Technol. Mater.*, 2023, **62**, 306–326.
2 S. Datta and S. Bhattacharya, *Chem. Soc. Rev.*, 2015, **44**, 5596–5637.
3 A. Pape, M. Bastings, R. Kieltyka, H. Wyss, I. Voets, E. Meijer and P. Dankers, *Int. J. Mol. Sci.*, 2014, **15**, 1096–1111.
4 S. Dhibar, H. Dahiya, K. Karmakar, S. Kundu, S. Bhattacharjee, G. C. Nayak, P. Karmakar, G. D. Sharma and B. Saha, *J. Mol. Liq.*, 2023, **370**, 121020.
5 K. Karmakar, A. Dey, S. Dhibar, R. Sahu, S. Bhattacharjee, P. Karmakar, P. Chatterjee, A. Mondal and B. Saha, *RSC Adv.*, 2023, **13**, 2561–2569.
6 S. Ganta and D. K. Chand, *Dalton Trans.*, 2015, **44**, 15181–15188.

7 G. Yu, X. Yan, C. Han and F. Huang, *Chem. Soc. Rev.*, 2013, **42**, 6697.
8 S. Dhibar, S. K. Ojha, A. Mohan, S. P. C. Prabhakaran, S. Bhattacharjee, K. Karmakar, P. Karmakar, P. Predeep, A. K. Ojha and B. Saha, *New J. Chem.*, 2022, **46**, 17189–17200.
9 M. Shirakawa, N. Fujita and S. Shinkai, *J. Am. Chem. Soc.*, 2003, **125**, 9902–9903.
10 T.-A. Asoh and A. Kikuchi, *Chem. Commun.*, 2012, **48**, 10019.
11 X. Yang, H. Zhang, J. Zhao, Y. Liu, Z. Zhang, Y. Liu and X. Yan, *Chem. Eng. J.*, 2022, **450**, 138135.
12 A. Rajak and A. Das, *ACS Polym. Au*, 2022, **2**, 223–231.
13 Y. Xu, Q. Wu, Y. Sun, H. Bai and G. Shi, *ACS Nano*, 2010, **4**, 7358–7362.
14 S. Dhibar, S. K. Ojha, A. Mohan, S. P. C. Prabhakaran, S. Bhattacharjee, K. Karmakar, P. Karmakar, P. Predeep, A. K. Ojha and B. Saha, *New J. Chem.*, 2022, **46**, 17189–17200.
15 J. W. Steed, *Chem. Soc. Rev.*, 2010, **39**, 3686.
16 K. Hanabusa, K. Hiratsuka, M. Kimura and H. Shirai, *Chem. Mater.*, 1999, **11**, 649–655.
17 B. Pal, S. Majumdar, K. Sundar Das, G. Lepcha, I. Pal, P. P. Ray and B. Dey, *J. Phys. Chem. Solids*, 2023, **182**, 111612.
18 S. Dhibar, B. Pal, K. Karmakar, S. Roy, S. A. Hafiz, A. Roy, S. Bhattacharjee, S. J. Ray, P. P. Ray and B. Saha, *Nanoscale Adv.*, 2023, **5**, 6714–6723.
19 B. Pal, S. Dhibar, R. Mukherjee, S. Bhattacharjee, P. P. Ray and B. Saha, *Mater. Adv.*, 2023, **4**, 3628–3635.
20 S. Dhibar, S. Pal, S. Some, K. Karmakar, R. Saha, S. Bhattacharjee, D. Kumari, A. Mohan, T. O. Ajiboye, S. J. Ray, S. Roy, S. Dam and B. Saha, *RSC Adv.*, 2025, **15**, 5214–5219.
21 C. Hu, X. Deng, X. Dong, Y. Hong, Q. Zhang and Q. Liu, *J. Membr. Sci.*, 2021, **619**, 118806.
22 J. J. Marrero-Tellado and D. D. Díaz, *CrystEngComm*, 2015, **17**, 7978–7985.
23 A. Prathap and K. M. Sureshan, *Langmuir*, 2019, **35**, 6005–6014.
24 N. Shi, G. Yin, H. Li, M. Han and Z. Xu, *New J. Chem.*, 2008, **32**, 2011.
25 S. J. Wezenberg, C. M. Croisetu, M. C. A. Stuart and B. L. Feringa, *Chem. Sci.*, 2016, **7**, 4341–4346.
26 M.-O. M. Piepenbrock, G. O. Lloyd, N. Clarke and J. W. Steed, *Chem. Rev.*, 2010, **110**, 1960–2004.
27 S. Dhibar, A. Dey, A. Dey, S. Majumdar, D. Ghosh, P. P. Ray and B. Dey, *ACS Appl. Electron. Mater.*, 2019, **1**, 1899–1908.
28 S. Dhibar, A. Dey, S. Majumdar, D. Ghosh, A. Mandal, P. P. Ray and B. Dey, *Dalton Trans.*, 2018, **47**, 17412–17420.
29 S. Ganta and D. K. Chand, *Dalton Trans.*, 2015, **44**, 15181–15188.
30 S. Naaz, P. Das, S. Khan, B. Dutta, S. Maity, P. Ghosh, P. P. Ray and M. H. Mir, *Polyhedron*, 2021, **201**, 115159.
31 C. Po, Z. Ke, A. Y. Tam, H. Chow and V. W. Yam, *Chem.–Eur. J.*, 2013, **19**, 15735–15744.
32 B. Jiang, L.-J. Chen, G.-Q. Yin, Y.-X. Wang, W. Zheng, L. Xu and H.-B. Yang, *Chem. Commun.*, 2017, **53**, 172–175.
33 C. A. Offiler, C. D. Jones and J. W. Steed, *Chem. Commun.*, 2017, **53**, 2024–2027.
34 Z. Yao, Z. Wang, Y. Yu, C. Zeng and K. Cao, *Polymer*, 2017, **119**, 98–106.
35 K. Mitsumoto, J. M. Cameron, R. Wei, H. Nishikawa, T. Shiga, M. Nihei, G. N. Newton and H. Oshio, *Chem.–Eur. J.*, 2017, **23**, 1502–1506.
36 Y. Lan, M. G. Corradini, R. G. Weiss, S. R. Raghavan and M. A. Rogers, *Chem. Soc. Rev.*, 2015, **44**, 6035–6058.
37 G. Deng, F. Li, H. Yu, F. Liu, C. Liu, W. Sun, H. Jiang and Y. Chen, *ACS Macro Lett.*, 2012, **1**, 275–279.
38 S. Das, M. Banik, G. Chen, S. Sinha and R. Mukherjee, *Soft Matter*, 2015, **11**, 8550–8583.
39 M. reza Saboktakin and R. M. Tabatabaei, *Int. J. Biol. Macromol.*, 2015, **75**, 426–436.
40 Y. Zhao, S. Song, X. Ren, J. Zhang, Q. Lin and Y. Zhao, *Chem. Rev.*, 2022, **122**, 5604–5640.
41 Y. Xu, Q. Wu, Y. Sun, H. Bai and G. Shi, *ACS Nano*, 2010, **4**, 7358–7362.
42 A. R. Hirst, B. Escuder, J. F. Miravet and D. K. Smith, *Angew. Chem., Int. Ed.*, 2008, **47**, 8002–8018.
43 S. Sarkar, S. Dutta, S. Chakrabarti, P. Bairi and T. Pal, *ACS Appl. Mater. Interfaces*, 2014, **6**, 6308–6316.
44 P. Terech, M. Yan, M. Maréchal, G. Royal, J. Galvez and S. K. P. Velu, *Phys. Chem. Chem. Phys.*, 2013, **15**, 7338.
45 C. Mahendar, Y. Kumar, M. K. Dixit and M. Dubey, *Soft Matter*, 2020, **16**, 3436–3442.
46 S. Dhibar, A. Dey, A. Dey, S. Majumdar, D. Ghosh, P. P. Ray and B. Dey, *ACS Appl. Electron. Mater.*, 2019, **1**, 1899–1908.
47 S. Dhibar, A. Dey, S. Majumdar, D. Ghosh, A. Mandal, P. P. Ray and B. Dey, *Dalton Trans.*, 2018, **47**, 17412–17420.
48 N. Maldonado and P. Amo-Ochoa, *Nanomater.*, 2021, **11**, 1865.
49 S. Dhibar, A. Dey, D. Ghosh, S. Majumdar, A. Dey, P. Mukherjee, A. Mandal, P. P. Ray and B. Dey, *ChemistrySelect*, 2019, **4**, 1535–1541.
50 K. Karmakar, A. Dey, S. Dhibar, R. Sahu, S. Bhattacharjee, P. Karmakar, P. Chatterjee, A. Mondal and B. Saha, *RSC Adv.*, 2023, **13**, 2561–2569.
51 S. Dhibar, S. Pal, K. Karmakar, S. A. Hafiz, S. Bhattacharjee, A. Roy, S. K. M. Rahaman, S. J. Ray, S. Dam and B. Saha, *RSC Adv.*, 2023, **13**, 32842–32849.
52 N. Malviya, C. Sonkar, R. Ganguly, D. Bhattacherjee, K. P. Bhabak and S. Mukhopadhyay, *ACS Appl. Mater. Interfaces*, 2019, **11**, 47606–47618.
53 (*a*) T. S. Rad, A. Khataee, E. S. Yazici, E. Gengec, M. Kobya and Y. Yoon, *Ultrason. Sonochem.*, 2025, **117**, 107351; (*b*) M. B. Hay and S. C. B. Myneni, *Geochim. Cosmochim. Acta*, 2007, **71**, 3518–3532.
54 D. Bairagi, P. Ghosh, P. Roy and A. Banerjee, *ACS Appl. Nano Mater.*, 2023, **6**, 2299–2309.
55 G. Lepcha, B. Pal, S. Majumdar, K. T. Ahmed, I. Pal, S. R. Biswas, P. P. Ray and B. Dey, *Mater. Adv.*, 2023, **4**, 2595–2603.
56 H. T. P. Anh, C.-M. Huang and C.-J. Huang, *Sci. Rep.*, 2019, **9**, 11562.
57 G. Lepcha, S. Majumdar, B. Pal, K. T. Ahmed, I. Pal, B. Satpati, S. R. Biswas, P. P. Ray and B. Dey, *Langmuir*, 2023, **39**, 7469–7483.

58 S.-Y. Chen, S.-T. Liu, W.-R. Lin, C.-K. Lin and S.-M. Huang, *Int. J. Mol. Sci.*, 2019, **20**, 5225.
59 C. Yu, J. He and J. Lu, *Small*, 2022, **18**, 2204023.
60 N. Malviya, C. Sonkar, R. Ganguly, D. Bhattacherjee, K. P. Bhabak and S. Mukhopadhyay, *ACS Appl. Mater. Interfaces*, 2019, **11**, 47606–47618.
61 Z. Lin, D. Han and S. Li, *J. Therm. Anal. Calorim.*, 2012, **107**, 471–475.
62 M. Z. Fahmi, M. Wathoniyyah, M. Khasanah, Y. Rahardjo, S. Wafiroh and A. Abdulloh, *RSC Adv.*, 2018, **8**, 931–937.
63 S. Anand, R. S. Sundararajan, C. Ramachandraraja, S. Ramalingam and R. Durga, *Spectrochim. Acta, Part A*, 2015, **138**, 203–215.
64 F. Bardak, C. Karaca, S. Bilgili, A. Atac, T. Mavis, A. M. Asiri, M. Karabacak and E. Kose, *Spectrochim. Acta, Part A*, 2016, **165**, 33–46.
65 F. Ahmad and A. Maqsood, *Phys. E*, 2022, **143**, 115353.
66 M. N. Ashiq, M. Javed Iqbal and I. Hussain Gul, *J. Magn. Magn. Mater.*, 2011, **323**, 259–263.
67 M. J. Iqbal and Z. Ahmad, *J. Power Sources*, 2008, **179**, 763–769.
68 S. Naaz, P. Das, S. Khan, B. Dutta, S. Maity, P. Ghosh, P. P. Ray and M. H. Mir, *Polyhedron*, 2021, **201**, 115159.
69 F. Ahmad and A. Maqsood, *Phys. E*, 2022, **143**, 115353.
70 V. S. Rai, D. Prajapati, V. Kumar, M. K. Verma, S. Pandey, T. Das, N. B. Singh and K. D. Mandal, *J. Mater. Sci.:Mater. Electron.*, 2022, **33**, 5273–5282.
71 S. Fares, *Nat. Sci.*, 2011, **03**, 1034–1039.
72 P. Das, B. Pal, J. Datta, M. Das, S. Sil and P. P. Ray, *J. Phys. Chem. Solids*, 2021, **148**, 109706.
73 P. Das, J. Saha, S. P. Pal, B. Pal, A. Layek and P. P. Ray, *J. Phys. Chem. Solids*, 2024, **188**, 111922.
74 S. K. Cheung and N. W. Cheung, *Appl. Phys. Lett.*, 1986, **49**, 85–87.
75 P. Das, J. Saha, S. P. Pal, B. Pal, A. Layek and P. P. Ray, *J. Phys. Chem. Solids*, 2024, **188**, 111922.
76 M. Tyagi, M. Tomar and V. Gupta, *Mater. Res. Bull.*, 2015, **66**, 123–131.
77 B. C. Roy, A. Kundu, P. Biswas, S. Roy and T. Singha Mahapatra, *ChemistrySelect*, 2024, **9**, 5.
78 S. Dhibar, A. Dey, A. Dalal, S. Bhattacharjee, R. Sahu, R. Sahoo, A. Mondal, S. Mehebub Rahaman, S. Kundu and B. Saha, *J. Mol. Liq.*, 2023, **370**, 121021.
79 L. Coppola, D. Coffetti and E. Crotti, *Constr. Build. Mater.*, 2018, **171**, 243–249.
80 A. A. Abdel Aziz, F. M. Elantabli, H. Moustafa and S. M. El-Medani, *J. Mol. Struct.*, 2017, **1141**, 563–576.